Heliyon 8 (2022) e08803

Contents lists available at ScienceDirect

Heliyon

journal homepage: www.cell.com/heliyon

Research article

Long-term power forecasting using FRNN and PCA models for calculating output parameters in solar photovoltaic generation

Hussein A. Kazem [a,b], Jabar H. Yousif [a,*], Miqdam T. Chaichan [c], Ali H.A. Al-Waeli [b], K. Sopian [b]

[a] Sohar University, PO Box 44, Sohar, PCI 311, Oman
[b] Solar Energy Research Institute, Universiti Kebangsaan Malaysia, 43600, Bangi, Selangor, Malaysia
[c] Energy and Renewable Energies Technology Research Center, University of Technology-Iraq, Iraq

HIGHLIGHTS

- Predict grid-connected PV system output using principal component analysis and recurrent neural approaches.
- Use one-year measured data to validating the proposed models.
- Evaluation and comparison of system performance using ANN models and experimental results.

ARTICLE INFO

Keywords:
Grid connected PV
Recurrent neural
Principal component analysis
Desert type PV
ANN

ABSTRACT

This paper evaluated a 1.4 kW grid-connected photovoltaic system (GCPV) using two neural network models based on experimental data for one year. The novelty of this study is to propose and compare full recurrent neural network (FRNN), and principal component analysis (PCA) models based on entire year experimental data, considering limited research conducted to predict GCPV behaviour using the two methods. The system data was collected for 12 months secondly and hourly data with 50400 samples daily. The GCPV evaluates using specific yield, energy cost, capacity factor, payback period, current, voltage, power, and efficiency. The predicted GCPV current and power using FRNN and PCA were evaluated and compared with measured values to validate results. However, the results indicated that FRNN is better in simulating the experimental results curve compared with PCA. The measured and predicted data are compared and evaluated. It is found that the GCPV is suitable and promising for the study area in terms of technical and economic evaluation with a 3.24–4.82 kWh/kWp-day yield, 21.7% capacity factor, 0.045 USD/kWh cost of energy, and 11.17 years payback period.

1. Introduction

Grid-connected photovoltaic (PV) systems have become one of the most attractive renewable energy applications. It is the most likely to replace a large part of fossil fuel energy. Many developments have taken places, such as improved performance of the PV module and lower costs. It is also highly flexible as it can be installed on the sea, valley, and mountains as well as in remote and desolate places where it is difficult for the electrical network to reach. Besides, it can be used in a hybrid system with wind and diesel energy systems [1]. One of the most critical barriers to the utilization of solar systems is the degradation of the performance of PV modules due to the impact of weather conditions (dust, solar radiation, ambient temperature, and relative humidity, etc.) [2]. PV module productivity decreases as cell temperature rise due to the absorption of most solar irradiance. It converts them into heat, leaving a small fraction only, which is converted to electricity. Dust accumulation causes low productivity and increases cleaning costs, as it is varied from one place to another. Also, the dust components depend on many parameters such as wind direction, the topographic and geological nature of the area, and human activities and pollutants. Researchers have suggested using photovoltaic thermal (PV/T) systems instead of separate thermal collector and PV modules as these systems cooled in different ways that increase their thermal and electrical productivity, respectively.

Many researchers have investigated and evaluated the electrical productivity of PV systems with varying grid-connected capabilities. Mishra et al. [3] used the deep learning and wavelet transform methods to predict PV power for a short-term period. The proposed model was validated using experimental data in Illinois. The proposed model

* Corresponding author.
E-mail address: jyousif@su.edu.om (J.H. Yousif).

https://doi.org/10.1016/j.heliyon.2022.e08803
Received 9 July 2021; Received in revised form 28 November 2021; Accepted 17 January 2022

achieved high performance based on evaluation factors that obtained RMSE of 0.0054, MAPE of 0.01906, MAE of 0.0381, and R^2 value of 0.66863. Shuvho et al. [4] evaluated and compared ANN and fuzzy logic prediction models to predict the energy produced by 80 kW PV power plants in Dhaka. The authors used data set from NASA and the two models compared with accuracy and error rate. The results confirmed that the ANN model is better than the Fuzzy model. Chbihi et al. [5] performed a comparative study of three different PV panels in two distinguished climatic stresses. The study examined the behaviors of the three separate panels and the various sites on the performance of PV panel production. Annual results record a loss between 0.44% and 1.1% on site—also, the other site lost between 1.8% and 5.9% for the three devices. Dahmoun et al. [6] examined and evaluated 23.92 MWp PV plants' performance in long-term (3-Year) located in El Bayadh, Algeria. The results confirmed the conformity of the desired data with the predicted data based on the high correlation coefficient of 91%. Wu *et al.* [7] proposed the use of a hybrid system called a thermoelectric system (PV-TE). In this system, the thermal generator connected to the back of the photovoltaic module converts heat into electricity depending on the temperature gradient between the two sides of the system. Charalambous *et al.* [8] and Kazem *et al.* [9] illustrated the importance of studying and predicting the power produced from PV/T systems before establishing large-scale PV power plants. There is also a need to improve models, technical and economic studies to estimate accurate results of these systems to enable significant changes to the future systems. Kotfas *et al.* [10] designed two photovoltaic systems of monocrystalline silicon and polycrystalline silicon panels connected to a thermoelectric generator on the hot side. The results of the study showed that the two studied systems caused a decrease in the temperature of the photovoltaic panels, which led to a clear increase in the generated power by about 11%. The best performance was when working with monocrystalline PV panels. This system was able to reduce the temperature of the panels by 6 °C at a solar irradiance of 440 W/m^2. The system also managed to reduce the temperature of the panels by 19 °C at an irradiance of 1000 W/m^2. Also, Mahmoudinezhad et al. [11] has studied numerically with empirical verification the behavior of a concentrated three-junction solar photovoltaic thermoelectric generator system. The study results showed that the energy produced by the studied system (a concentrated three-junction solar cell) changed rapidly with the change in the solar radiation intensity, but this change became gradual when using the thermoelectric generator due to its thermal capacity and resistance. Therefore, the study found that the adoption of the thermoelectric generator in the thermoelectric solar cell system provides a stable generation power.

Machine learning based on artificial neural networks (ANN) has been used in many applications, including data recognition and classification, future value prediction, control systems, and operation. ANNs are mathematical algorithms that mimic the functions of the human brain. The neural network processes inputs and can handle them based on its structure. The use of intermediate neurons in the hidden layer reduces errors and accelerates the learning process by adjusting the weight of each neuron with the reconstruction of new weight values. The ANN is classified into two types based on how the signal moves from the input to the output layer (feedforward and feedback-recurrent-) [12]. Wu *et al.* [13] examined the potential of the ANN technique compared to practical results and used to predict the performance of solar PV systems. The researchers concluded that predicting the productivity of PV plants based on the ANN concept is well-fitting the desired data. Cooling is used to improve the performance of photovoltaic cells by switching to PV/T systems, so that, Al-Waeli *et al.* [14] developed three models of linear prediction and compared them to ANN models to predict the productivity of PV/T system cooled by (nano-SiC-water) nanofluid and nano-SiC-paraffin wax (PCM). The result's accuracy was verified by comparing them with experimental results. The study results showed that the linear prediction algorithms studied reduced the error rate in the predicted results and can contribute to determining the best-operating conditions for any PV system easily and quickly.

The concept of deep learning (recurrent neural) is based on an automatic learning mechanism to represent data by spreading a multi-layered neural network. These classes are classified into uncensored, semi-controlled, and supervised [15]. The "deep learning" concept is used first to find out if there is any defect in the network. This concept is a combination of deep learning geometry, wavelet transformation, and a multi-precision mono universe. This concept has the potential to achieve the desired goal with high accuracy [16]. Hossain *et al.* [17] used deep learning to predict the output of a PV system and compared the results with the outcomes of other studies that have adopted various methods such as an artificial neural network (ANN) and support regression vectors (SVR). The study results confirmed high prediction accuracy of energy generated by the used PV system and at a less computational time could be achieved using deep learning. Du Plessis et al. [18] proposed hybrid neural models using macro-level deep learning neural networks, Long Short-Term Memory, and recurrent neural techniques for forecasting a short-term power of a 75 MW grid-connected PV system. The results show that the proposed model achieved the best mean absolute percentage error (MAPE), varying between 1.42%–8.13%, which concluded that the proposed models could capture the low-level behavior of the PV system.

Many researchers have shifted to the use of deep learning in the study of PV systems and to predict their productivity; for example, Wang *et al.* [19] proposed three neural networks for deep learning to predict the output of a PV plant. The researchers selected the most suitable algorithm, which showed the best predictability of the power produced by the station studied. Wen *et al.* [20] used the deep-learning concept to predict the PV system's output used for domestic purposes. The researchers suggested that the proposed method may outperform other methods and advised to use it to predict microgrid systems as it contributes to reducing the cost by 8.97%. Talaat et al. [21] proposed a multilayer feedforward neural network (MFFNN) optimization model based on multiverse Optimizer (MVO) and genetic algorithms (GA) to forecast the PV power output of the 4-kW PV plant installed in Shaqra City, Saudi Arabia. The three parameters were deployed for training and testing the Neural proposed model: ambient temperature, wind speed, and solar irradiance. They examined the efficiency of PV using the normalized root mean square error and obtained a rate of 3.65E-4 and 2.82E-4 for MFFNN-GA and MFFNN-MVO models. Qu et al. [22] deployed a neural temporal distributed model based on recurrent deep learning for predicting the PV power generation for a panel installed in a farm in southeastern China. Also, proposed an ARIMA linear forecasting model for forecasting the linear series data at each linear trend segment. The proposed model achieved high performance with an accuracy of 62.7%. And less nominalized root mean square error of 0.083 and a nominalized mean absolute error of 0.041. Chahboun & Maaroufi [23] deployed a Principal Component Analysis to compare the performance of several machine learning approaches to predicate the PV power production. The comparison includes the Bayesian regularized neural, elastic net, support vector machines regression, and random forest networks. The results show that the Bayesian neural model achieved the highest accuracy of 99.9% and RMSE of 0.002. It follows by the Random Forest regression with an RMSE of 0.1434 and accuracy of 99.53%. Sun *et al.* [24] asserted that for short-term solar prediction, it is appropriate to use a convolutional neural network characterized by precise regulation of hybrid input and chronological date. The use of deep learning outperforms the stability model by 15.7–16.3%. Depending on the input (celestial images) and the output of the efficient PV system, the training time was reduced up to 83.0% without affecting the accuracy of the

predicted results. Another prediction method is the principal component analysis (PCA), a crucial category of unsupervised learning methods, aiming to dimensionality-reduction multi domination input space.

This study aims to evaluate the potential of grid-connected PV systems in Oman using recurrent neural and principal component analysis models. GCPV systems. Limited studies used the two methods to investigate GCPV systems. Also, the current paper compared the two methods results with the experimental values. For this purpose, a 1.4-kilowatt grid-connected PV plant was installed in the northern city of Oman, Sohar. To assess the performance of the system, weather data, and system outputs (current, voltages, and power) were collected for an entire year from July 2018 to the end of June 2019. Predicting the productivity of a PV plant has become a very active research area. It helps to accurately predict and give data on the power of the plant with its secure connection to the central power grid. References [22, 23, 24, 25, 26, 27, 28] have demonstrated that the adoption of recurrent neural algorithms can safely predict the conditions and productivity of grid-connected PV plants. Unfortunately, to date, only a minimal method of recurrent neural has been applied to predict the results of grid-connected PV systems.

The main contributions of this paper are to evaluate and comparative analysis of the grid-connected PV system performance in Oman. Experimental evaluation in terms of technical and economic aspects is presented first. The innovative aspect consists of proposed recurrent neural and principal component analysis ANN models based on an entire year of collected data. These models help to reduce the operational costs of these power plants. Many research studies confirmed ANN models as an excellent predicting approach. Unfortunately, a few research works conducted the use of FRNN and PCA to PV output prediction. In these models, analyzed data previously obtained to predict the relationship between the input and output of the grid-connected PV system. These models are sophisticated, and their applications are especially useful for incomplete data and result in optimal learning models. The improvement in the proposed model is not just about adopting training data but also adopting the data that is best anticipated for system productivity.

2. Methodology and experimental setup

2.1. PV system description

Grid-connected PV systems (GCPV) consist of ten 140 GH-2PU PV modules and an inverter have been installed to equip electrical peak power up to (1.4 kW) with a generated voltage of (177 V DC) under standard test conditions each (Figure 1) at Sohar University, north of Muscat. This system is installed in the Sohar University campus, for scientific research purposes. The PV modules are installed at a fixed optimum tilt angle (27° facing southward depending on Kazem et al. results) [31]. The PV modules are connected in series to supply sufficient voltage to the grid-connected inverter (the ten connected PV modules provided a series of 177 V). The inverter used is a Sunny Boy 1700 type (1.5 kW, 220–240 AC voltage, and 94.2% efficiency). Also, the PV module short circuit current and open circuit voltage are 8.68 A and 22.1 V, respectively. However, the highest PV and inverter efficiencies are 13.9% and 94.1%, respectively.

Figure 1. GCPV system.

Table 1. Experimental setup accessories and uncertainty.

Sensors and measuring instruments		Experimental uncertainty
Thermocouples	Qt. 24, K-type	±1.09 °C
Pyranometer (Global irradiance)	Apogee, (0–1300) W/m^2	±1.20%
Flow meter (heat resistence)	0.01–0.30 kg/s	±0.22
Anemometer cup	0–5 m/s	±1.00%
Data-logger and software	Capture data	
PV kWh metre	Display and logging data	
Laptop	Data storage	

The system was equipped by many thermocouples to measure the modules temperature, pyranometer to measure the global irradiance, and anemometer to measure the instantaneous wind speed. The system also was attached to a data logger and software to catch the data. PV kWh meter to display the logging data, and a laptop to store the gathered data.

All measuring instruments and devices were calibrated before use. Table 1 lists the above systems description and uncertainty.

2.2. Study area

The study was conducted in Oman, which is one of the Middle East countries that fall within the solar belt [26]. Oman relied heavily on natural gas and diesel for electricity production [38]. There was no share of renewable energy in the energy supply despite several resources, including solar, wind, and hydropower [33]. Over the past few years, electricity consumption in Oman has risen dramatically. In 2000, the country's electrical energy consumption was 6850 GWh, while in 2018, it reached 27,620 GWh [34]. All sectors, including residential, commercial, and industrial consumption, increased during this period. Oman has enormous solar potential as the solar irradiation arriving in this country is one of the highest in the world [35]. Oman receives solar irradiance ranging from 2500 to 3000 W/m^2/day in January, rising to 5500–6000 W/m^2/day in July [34]. With the proliferation and success of GCPV systems in the Gulf Cooperation Council (GCC) region and within Oman's energy vision in 2040, several gigawatts of electricity were planned to be produced using PV plants.

Sohar is one of the northern provinces of Al-Batinah and is located in the northern part of Oman. Also, Sohar is 234 km north of the capital Muscat [31]. Figure 2 shows ambient temperature, diffuse and global solar irradiance. The daily average diffuses and global solar energy for the city of Sohar is 3289 Wh/m^2/day and 6182 Wh/m^2/day, respectively. This potential of solar irradiance illustrates an excellent solar energy zone, which motivates PV systems investments.

The average daily ambient temperature in the study area is moderate (32 °C), and wind speed 4.4 m/h southeast, and the average relative humidity is 40%. These values show the suitability of the study area to install PV systems, where the average temperature and wind speed are suitable for cooling PV panels, while the relative humidity is not high in a way that causes negative effects on these systems.

2.3. Performance evaluation criteria

GCPV systems evaluation criteria were defined by the “International Electro-technical Commission IEC61724”. The criteria contain energy production (E) and yields (SY), performance ratio (R), cost of energy (CoE), life cycle costs (LCC) and recovery period (PBP), present worth (MC), the percentage value of the replacement cost (RC), efficiencies (η), losses (P_{loss}) and capacity factor (CF) [24, 25, 32]. These criteria defined in Table 2, respectively.

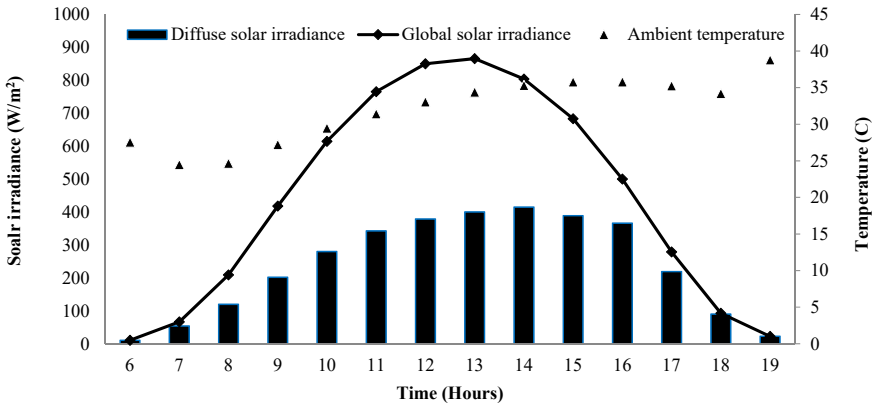

Figure 2. Sohar profiles for solar irradiance and ambient temperature.

Table 2. The used equations for PV-generated power and performance evaluation criteria.

Parameters	Eq. #	Parameters	Eq. #
$YF_d = \frac{E_{PV}(kWh/year)}{PV_{WP}(kWp)}$	(1)	$MC_{0r} = k_r \times IC_r$	(6)
$YF_F = \frac{E_{AC}(kWh/year)}{PV_{WP}(kWp)}$	(2)	$MC = \sum_1^r MC_r$	(7)
$YR = \frac{G_T}{G_{STC}}$	(3)	$RC_k = IC_k \times \sum_{j=1}^{N_r}\left(\frac{1+FR}{1+IR}\right)\left(\frac{LP \times j}{N_r+1}\right)$	(8)
$CF = \frac{SY}{8760} = \frac{E_{PVannual}}{(P_R \times 8760)}$	(4)	$RC = \sum_{k=1}^{2} RC_k$	(9)
$PR = \frac{SY}{Y_R}$	(5)	$CoE = \frac{LCC}{\sum_1^n E_{PV}}$	(10)
$LCC = C_{capital} + \sum_1^n C_{O\&M}.R_{PW} + \sum_1^n C_{replacement}.R_{PW} - C_{salvage}.R_{PW}$			(11)
$R_{PW} = F/(1+i)^N$	(12)	$P_{PV}(t) = P_{peak}\left(\frac{G(t)}{G_{stc}}\right) - \alpha_T[T_c(t) - T_{stc}]$	(14)
$C_{capital} = CA_i \times UC_i + ICI$	(13)	$T_c(t) - T_{amb} = \left(\frac{NOCT-20}{800}\right)G(t)$	(15)
$MC_r = MC_{0r} \times \left(\frac{1+f}{i-f}\right) \times \left[1 - \left(\frac{1+f}{1+i}\right)^N\right]$			(16)
$E_{AC,t1} = \sum_{t=1}^{N} E_{AC,t2}$	(17)	$\eta_{sys} = \frac{E_{AC}}{G(t) \times A_c} \times 100\%$	(18)
$\eta_{PV} = \frac{E_{DC}}{G(t) \times A_c} \times 100\%$	(19)		

The definition of specific yield or factor (SY or YF) is "the annual, monthly or daily net AC energy output of the system divided by the peak power of the installed PV array at standard test conditions (STC)". Where: YF_d represents array yield while YF_F is final yield and Y_R is references yield. Also, the capacity factor (CF) estimates benefits obtained from the system. It is known as: "the ratio of the actual annual energy output to the amount of energy the PV array would generate if it were operated at full rated power (P_R) for 24 h per day for a year". The performance ratio definition (P_R) is "the standard employed to evaluate the used PV system quality". Life cycle cost "LCC" is the sum of the capital cost ($C_{capital}$) plus all present costs (R) minuses ($C_{salvage}$), which is evaluated by the Eq. (11). The energy cost is calculated using LCC and E_{PV} as in Eq. (10), and the PV-generated power is calculated in Eq. (14). The T_c is calculated as in Eq. (15). Also, the PV electrical energy generated is calculated in Eq. (17) in a set of periods (hour, day, or month). N = 60 min, 24 h, and 30 days for an hour, day, and month, respectively. Finally, Eqs. (18) and (19) calculate PV array and system efficiencies. E is energy in Wh, G irradiation in Wh/m^2, and A is the PV area in m^2 as presented in Table 2.

3. Neural computation architectures

The artificial neural network (ANN) simulates linear or nonlinear relationships and reduces complex data associations' dimensionality. ANN is a computational mathematical function based on symbolic rules

Table 3. The specification of proposed neural network models' structure.

Model	#Input variables	#Hidden Layers	#Output Variables	#Epoch	Activation Function	Learning fuction
FRNN	Temperature (oC) solar irradiation (W/m^2)	1, 2, 3 Best (1)	Current (mA) Voltage (V) Power (W)	100, 500, 1000 Best (1000)	TanhAxon	momentum $\alpha = 0.7$
PCA	Temperature (oC) solar irradiation (W/m^2)	1, 2, 3 Best (1)	Current (mA) Voltage (V) Power (W)	100, 500, 1000 Best (1000)	TanhAxon	momentum $\alpha = 0.7$

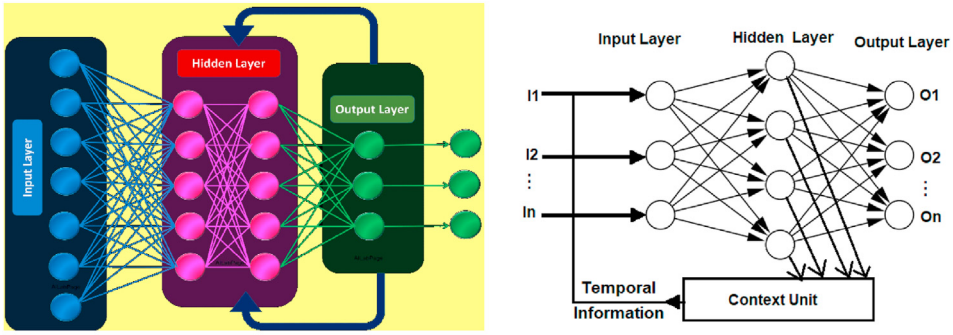

(a) (b)

Figure 3. Artificial Neural Architecture. (a) Recurrent Neural Network; (b) PCA network Architecture.

that emulate biological brain activities and mimics intelligent human behaviour. The unique features of ANN like parallelism computing, generalization, recurrent computing, and learning from experience made it a proper approach for utilizing in many applications such as classification, recognition, and association of data, etc.

Several architectures of ANN were developed and deployed for monitoring and assessing the behaviour of renewable production systems. Several models utilize an internal memory for saving the updated context information using past observations. Heterogeneous neural models combined the feedforward and feedback mechanism to simulate the recurrent neural system creating at any layer [36]. The accurate predicting and examining solar irradiance are required in setting up and sizing solar power applications. Therefore, finding robust mathematical is crucial to control and manage the electrical grid effectively. Artificial Neural Network (ANN) can provide manageable and accurate prediction models with less computational effort. It can train with a minimum number of datasets and control uncertainty in resource computation, which helps enhance the forecasting models' performance. In addition, the use of hidden layers and recurrent approach helps to improve the results and fits the actual data. Also, the ANN provides a robust sensitivity analysis of input variables for the best selection variables that increase the model performance. The neural network implementation of Principal Component Analysis (PCA) and Full-Recurrent Neural (FRNN) algorithms were deployed using the NeuroSolutions software package [37]. Table 3 shows the structure of both proposed methods (FRNN: 2-1-3, and PCA: 2-1-3), which means it consists of 2 inputs layers, 1 hidden layer, 3 output layers.

3.1. Recurrent neural network (RNN)

Recurrent Neural Network (RNN) computationally is more effective than feedforward networks because it mimics the human biological nature because it will use inputs that have already been processed and reused again to correct errors, as shown in Figure 3(a).

Many recent studies [18, 28, 29, 30, 38, 41] deployed and confirmed the high efficiency of the RNN network compared to traditional ANN in diverse applications. It is mainly used in applications that require remembering to keep the sequence of input patterns based on the time interval. The Full recurrent neural (FRNN) is a mathematical model that processes the input datasets with a recurrent cycle of sending the outputs of the hidden layer to feedback as input in the next stage. The production of hidden layers will pass to the output layers, which will feedback the output results as input again and forth until the stability of the activated layers, whether hidden or output — the backpropagation learning through time (BPTT) utilizing the gradient error to adjust the neuron weight [38]. BPTT was used to remember previous information and store and record it in long-term memory (LSTM). A reparative process is used to adjust the values of the weights in the network. The adjustment process computes the activation function in the hidden layers until the network is stabled.

The recurrent neural networks (RNN) deployed leverage back-propagation through time (BPTT) algorithm to determine the gradients in less time compared to the traditional method. It can measure the input data in time series that each input sample can be dependent on previous values. It can remember the last data for a long time, which helps to determine their Default behavior. Therefore, RNN can speed the predication computation and getting the results.

Back propagation learning method processes the information in both feedforward, and backward directions to reduce the error of the network, which passed back the information to the next layer through the links [38]. The BP method adjusts and utilizes the weights' values of neurons as defined in Eq. (20):

$$\mathrm{E(w)} = \sum_{p=1}^{pt} \sum_{i=1}^{epoch} (\mathrm{di(p)} - \ \mathrm{yi(p)})^2 \tag{20}$$

The current neuron weight is computed as in Eq. (21):

$$Wij(n+1) = Wij(n) + \eta\delta i(n) + xj(n) \tag{21}$$

The momentum rule utilizes to accelerate and adjust the value of neurons weights, which is defined in Eq. (22):

$$Wij(n+1) = Wij(n) + \eta\delta i(n) + xj(n) + \alpha(Wij(n) - Wij(n-1)) \tag{22}$$

Where the step size (η) sets to 0.7 [36].

3.2. Principal component analysis (PCA)

PCA is a crucial category of unsupervised learning methods, which aims to dimensionality-reduction of multi domination input space. PCA process the input space for computing a set of orthogonal directions (eigenvectors of the correlation matrix) and produce projections (the corresponding eigenvalues) of ordered directions [39]. Many of the features that motivate researchers to use PCA, which include diminishing dimensions to reduce training time and use suitable representations, may enhance model performance. Therefore, it reduces the high dimensionality of the input data to a low dimensionality of the input data, which will help to speed the computation and improve the prediction model's performance. Figure 3(b) shows the PCA architecture, which is determining the eigenvalue using the correlation ship method.

The score matrix of PCA is computed as in Eq. (23):

$$y_{ij} = w_{1i} \times x_{1j} \ + w_{2i} \times x_{2j} + w_{pi} \times x_{pj} \ \ \ldots \tag{23}$$

where w is the matrix of weights, and x is the data matrix of n observations and p variables.

The w matrix is calculated using the variance-covariance matrix (s) as in Eq. (24)

$$S_{ij}=\frac{\sum_{k=1}^{n}\left(x_{ik}-\bar{x}_i\right)\left(x_{jk}-\bar{x}_j\right)}{n-1} \quad (24)$$

The correlation relationship between the i^{th} factor and the j^{th} variable is determined as in Eq. (25).

$$r_{ij}=\frac{u_{ji}{}^{*}\sqrt{l_i}}{S_{jj}} \quad (25)$$

Several factors are implemented for assessing the accuracy of the output of proposed models. "Coefficient of determination (R^2)" is the most momentous method uses to evaluate the performance of predicting models as defined Eq. (26).

$$R^2=1-\frac{\sum_i^n\left(y_i-p_i\right)^2}{\sum_i^n\left(y_i-\overline{y}_i\right)^2} \quad (26)$$

Where y_i is the estimated output, p_i is the predicted output and is the arithmetic mean value of y_i. Besides, methods like "Mean Square Error (MSE)", "Root Mean Square Error (RMSE)", "Mean Absolute Error (MAE)" and "Mean Absolute Percentage Error (MAPE)" are broadly used to measure and validate the results of mathematical and predicting models as resulted from Eqs. (27), (28), (29), and (30), respectively.

$$MSE=\frac{1}{N}\sum_{i=1}^{N}\left(p_i-y_i\right)^2 \quad (27)$$

$$\mathrm{RMSE}=\sqrt{\frac{1}{N}\sum_{i=1}^{N}\left(y_i-p_i\right)^2} \quad (28)$$

$$MAE=\frac{1}{N}\sum_{i=1}^{N}\left|p_i-y_i\right| \quad (29)$$

$$MAPE=\left(\frac{1}{N}\sum_{i=1}^{N}\left|\frac{y_i-p_i}{y_i}\right|\right)*100 \quad (30)$$

The normalized mean square error calculates the mean relative scatters and reflects the random error, ensuring that the results of the predictions will not be biased in overestimated or underestimated cases. It is computed in the equation Eq. (31).

$$\mathrm{NMSE}(x,y)=1-\frac{\left|\left|(x-y)\right|\right|^2}{x-\bar{x}} \quad (31)$$

$\bar{x}=\frac{1}{N}\sum_{i}^{n}(x_i)^2$; where y is the approximation to x.

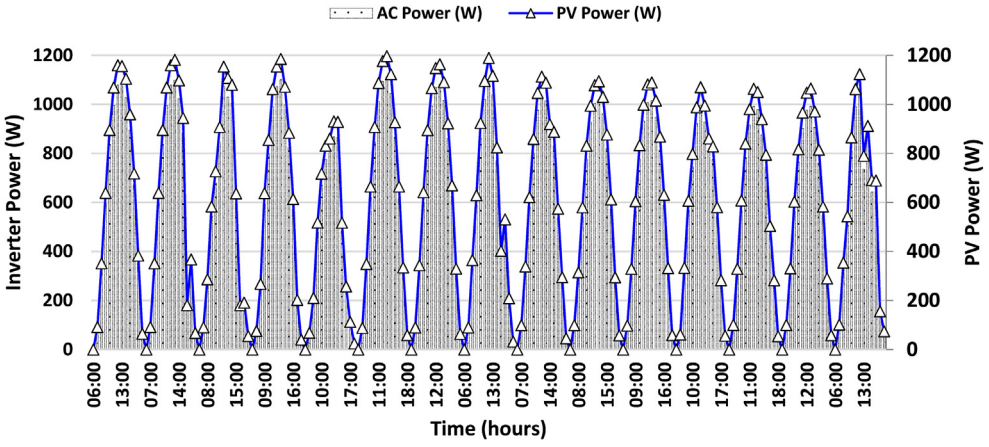

(a)

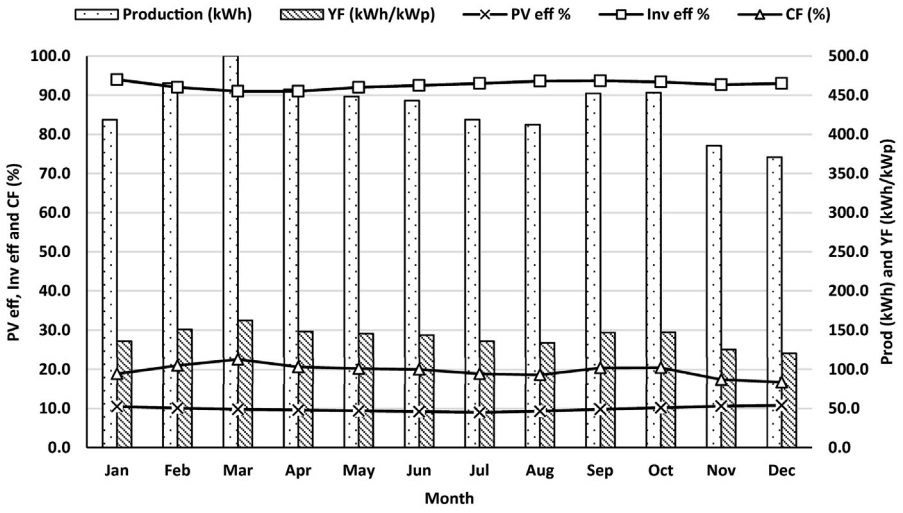

(b)

Figure 4. (a) PV and Inverter power production (1–15 April 2019); (b) GCPV technical performance parameters for entire year.

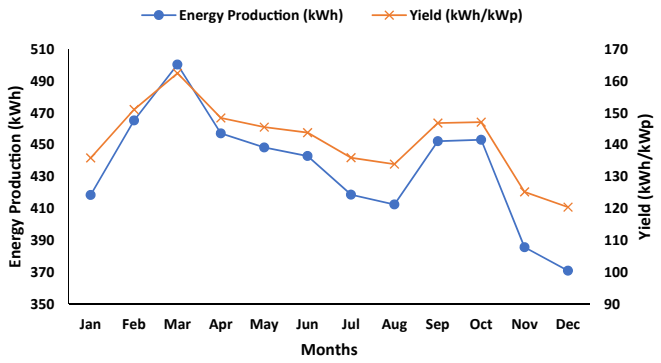

Figure 5. Grid-connected PV system and monthly performance.

4. Results and discussion

4.1. Experimental results

The GCPV system's electrical and environmental data were measured and recorded to analyze the performance. The sensors record every second and hourly data used for long periods. However, the data was used to investigate the system performance for 1, 15, and 365 days. Figure 4 (a) illustrates PV and Inverter powers for the period from 1 to 15 April 2019. Because the Inverter efficiency is relatively high (94.5%), so the conversion losses from DC to AC are low.

In addition, the energy production (P_{PV}) is generally high even though April is a spring season in the study area where the climate is moderate in the shade, and the intensity of the sun is less variable than in summer. Throughout the year, the best time for intensity and P_{PV} was summer (May–October) with 245.8 kWh in June, when the sun-directed illumination is moderately higher and reflectively reflected on the PPV. Similarly, the lowest power and PPV recorded was in winter (November to February) with 224.5 kWh in February.

Figure 4 (b) demonstrates the variety of deliberate PPV, PV energy (EPV), and global solar radiation (G) of a specified day (1 June 2019). The highest values for G are in June during the day, and PPV is 1158 W. Be that as it may, the temperature is moderately high, which diminishes P_{PV} and efficiency. The P_{PV} and E_{PV} bend depends upon *G*, and they are in consistence with more smooth energy bend early morning and late evening. This circumstance is because of the variety in temperature and *G* in these periods. Also, for the entire year, it is found that the GCPV array, reference, and final yields (*YF*) varied in the extent of 3.43 to 5.65 kWh/kWp-day, 4.61 to 7.33 kWh/kWp-day, and 3.24 and 4.82 kWh/kWp-day, respectively. Since *G* is high, *YF* is high too, where they are in directional proportionality. However, *YF* shows a significant consistency with the systems in literature [41, 42, 43]. Also, *CF* was 21.7%, *CoE* was 0.045 USD/kWh, and *PBP* is 11.17 years, calculated for the system. It is worth mentioning that *CF* is close to the typical 21%, and the *PBP* is promising. Furthermore, the *CoE* is interested since it is cheaper than using natural gas to generate electricity in Oman, where *CoE* is 0.180 USD/kWh (without government subsidies). The GCPV efficiency fluctuated between 9.1% and 10.8% — likewise, the most extreme efficiency was

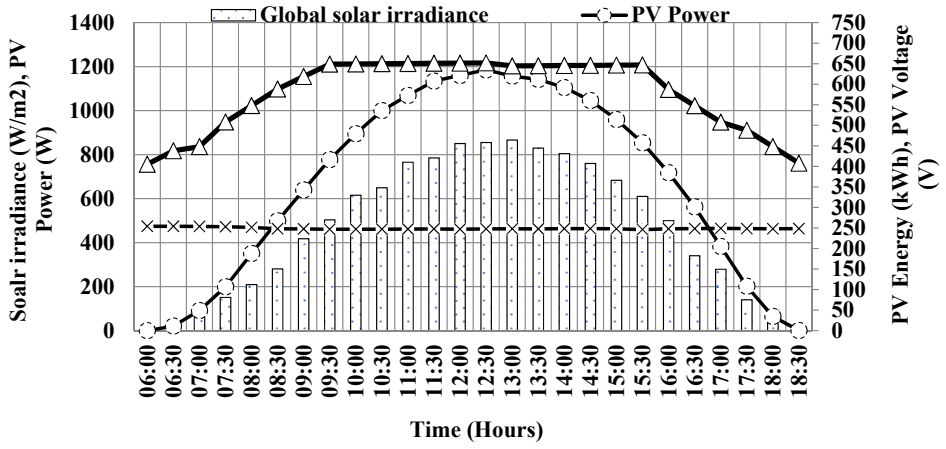

Figure 6. PV system power, energy, voltage, and solar irradiance.

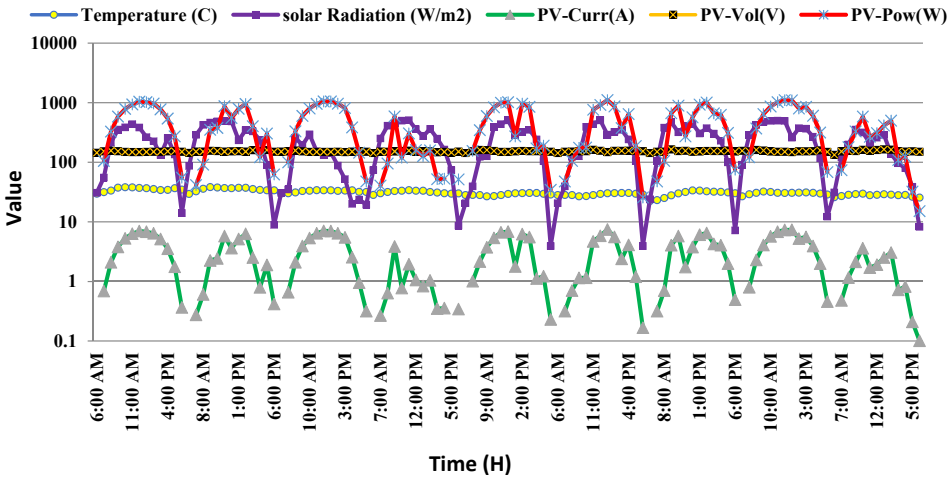

Figure 7. The relation between the input variables (ambient temperature, solar irradiance.) and output variables (power, voltage, current).

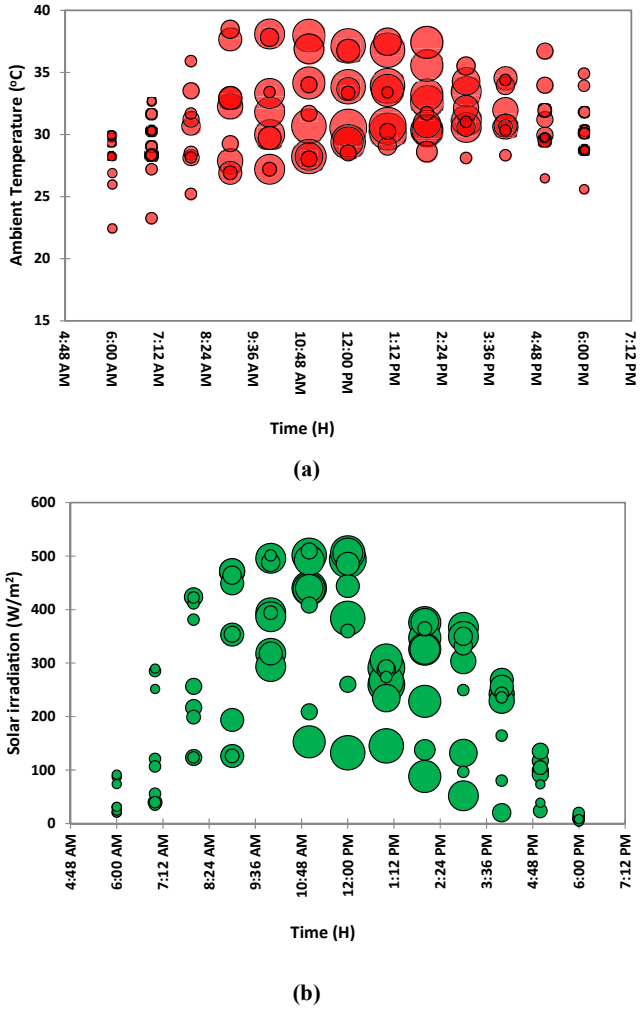

Figure 8. Scatter plotting method of the variable (a) ambient temperature; (b) solar irradiation.

found in December while the least efficiency was in July. It is known that the solar radiation is higher in July than in December, yet the climate is increasingly dusty and hotter in July, which will adversely affect P_{PV}, *YF*, *CF*, and efficiency this month (see Figure 5). Also, inverter efficiency improved from 91% to 94%.

The yearly normal of the performance ratio observed to be 0.67 different between 0.53 in June and 0.71 in January. The performance is highly dependent on the season, either summer or winter, given the temperature and P_{loss} in summer are positively different to circumstances in winter.

The GCPV system AC voltage is delineated in Figure 6, which shows high consistency. Based on measured values, it is found that the normal every day AC voltage and frequency are 49.98 Hz (±0.02%) and 248.58 V (±0.21%), which agree to power guideline in Oman.

Likewise, GCPV current estimated and recorded each second and found to be consistent and follow *G* curve, with the highest current 7.70 A at noon.

4.2. ANN experimental implementation

The experiments utilize different recurrent neural approaches, including Principal Component Analysis (PCA) and Full-Recurrent Neural approaches (FRNN). The NeuroSolutions software package is used to design and implement the current proposed neural models. The experimental data were collected in Sohar city (Coordinate: 24.3501° N, 56.7133° E) Oman, which recorded a data set everyone hour. However, the data used to investigate 1, 15, and 365 days, and Inverter powers for the period 1–15 April 2019. Two main factors should be chosen carefully to enhance network output performance (number of epochs and hidden layers). The experimental data consists of 500 datasets that are used for training and testing the proposed models. 60% datasets are used in the training phase and 20% of datasets for the cross-validation phase, and 20% of datasets for testing the results. Different epochs (100, 500, 1000) are tested to choose the optimal number of epochs that maximize network performance and reduce the MSE error. The maximum number of epochs is 1000. Also, the number of hidden layers determined according to the experimental data sets, which are set to one and two layers. The number of hidden layers must be set between the number of input variables and the outputs [40]. The experiments utilized the network architectures using two input variables (ambient temperature and solar irradiation). Also, the output variable is Experiment 1 and Experiment 2, which is assigned either to PV current (*I*) or power (*P*), respectively. Input variables for the FRNN models are temperature ambient and solar irradiance. The output of Experiment 1 is the Current (I), while the output of Experiment 2 is the Power (P). Also, Input variables for the PCA models are temperature ambient and solar irradiance. The output of Experiment 1 is the Current (I), while the output of Experiment 2 is the Power (P). The transfer function is TanhAxon, the number of epochs is 100, 500, and 1000, the learning algorithm is momentum $\alpha = 0.7$ with a step size of 1, and the number of data sets is 500 pair (300 datasets for training, 100 datasets for cross-validation, and 100 datasets for testing). The proposed neural models were performed under the same conditions for systematic analysis. However, the number of hidden layers is two and one for FRNN and PCA, respectively.

4.2.1. Statistics results

Figure 7 shows the relation between the experimental data of the input variables (ambient temperature, solar radiation) and the data of output variables (power, voltage, current). The figure shows some differences in the curves of input-output variables between 0 and 1200. Therefore, the variables (such as voltage and ambient temperature) with a low amount and variation are close to the horizontal axes (time). It is found from Figure 7 that the current waveform is more consistent with G

Table 4. Descriptive statistics data of quantitative variables.

	Ambient Temperature (°C)	Solar irradiation (W/m²)	Current (A)	Voltage (V)	Power (W)
Mean	31.19	236.90	2.79	152.71	428.64
Median	30.63	249.38	2.09	152.32	327.31
Standard Deviation	3.28	159.95	2.41	4.66	365.60
Kurtosis	-0.1201	-1.2817	-1.2334	2.2020	-1.3033
Skewness	+0.2227	+0.0965	+0.4882	-0.1542	+0.4382
Minimum	22.44	3.9200	0	133.7600	0
Maximum	38.45	509.45	7.46	164.81	1106.35
Sum	3650.33	27717.61	327.54	17868.05	50151.97
Count	117	117	117	117	117

Table 5. Correlation matrix of quantitative variables.

Variables	Ambient temperature (°C)	solar irradiation (W/m^2)	Current (mA)	Voltage (V)	Power (W)
Temperature (°C)	1.0000	0.3492	0.3997	0.0131	0.3926
solar irradiation (W/m^2)	0.3492	1.0000	0.5244	0.2951	0.5324
Current (mA)	0.3997	0.5244	1.0000	0.0993	0.9993
Voltage (V)	0.0131	0.2951	0.0993	1.0000	0.1270
Power (W)	0.3926	0.5324	0.9993	0.1270	1.0000

comparing with other waveforms. However, the power followed the current pattern and it is affected more by current variation in terms of wave shape. On the other hand, the voltage values had more impact on power production.

Figure 8 (a and b) depicts a definite figure of the form of ambient temperature and solar irradiance using a scatter plotting method, respectively. This figure illustrates the pattern and data analysis for *T* and *G*. The maximum amount of temperature is 38.4 °C at 9:00 AM. Also, the minimum value of temperature is 22.4 °C at 6:00 AM. However, the data concentrated at 32.5 °C. Also, it records that the minimum value of solar irradiance is 3.9 W/m^2 at 6:00 PM, while the maximum amount is 509.4 W/m^2 at 11:00 PM, with data concentrated at 343.6 W/m^2. However, it observed that there is some consistency between solar radiation and PV current. The data was collected using sensors, data acquisition and monitoring systems. It should note that uncertainty is very limited in this study due to the large number of

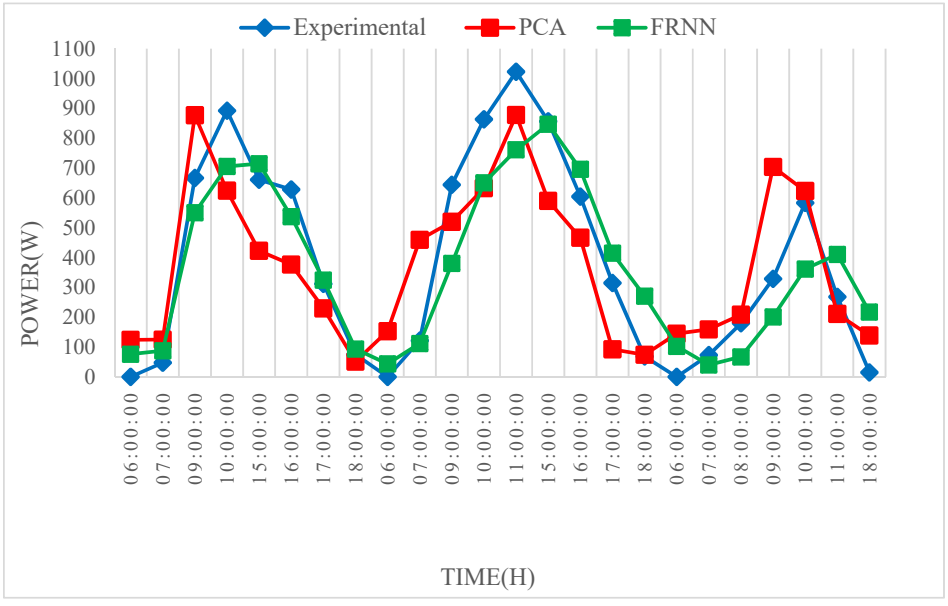

(a)

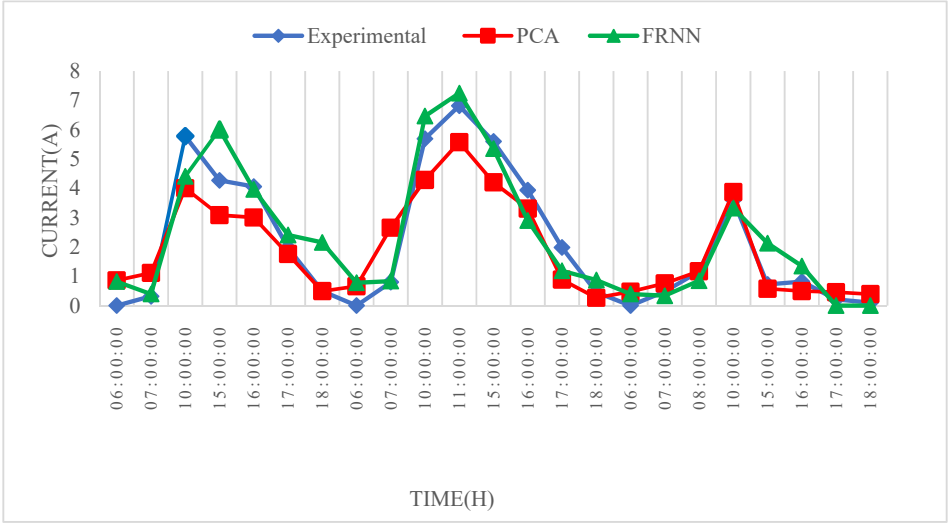

(b)

Figure 9. A comparison of the experimental data and the predicted output of proposed models (FRNN, PCA). (a) Power data; (b) Current data.

Table 6. The evaluation factors and results of proposed neural models.

	Power		Current	
	FRNN	PCA	FRNN	PCA
MSE	0.1778	0.0780	0.0488	0.0768
NMSE	0.4965	0.4391	0.4434	0.4420
R^2	0.7471	0.7533	0.8119	0.7623

measured data (50,400 values), which was taken at 14 h a day, making it easier to validate the results.

4.2.2. Skewness and kurtosis results

Skewness and kurtosis are two proper functions measure of symmetry for explaining the descriptive statistics data, which depicts the configuration of the data distribution. Skewness assesses the degree of symmetry in the distribution of the dataset. Datasets have symmetrical (normal) distribution if the value of Skewness is equal to 0. Skewness estimates the comparative size of the two tails. The Skewness is computed as in Eq. (32). Kurtosis is used to determine the probability at the merged scales of the two tails as defined in Eq. (33). If the value of the kurtosis is equal to 3, then the datasets follow a normal distribution. Also, the dataset will have more massive tails if the value of kurtosis is greater than 3. Also, the dataset will have lighter tails than a normal distribution if the value of kurtosis is less than 3.

$$skew\ a_3 = \sum \frac{(x_i - \overline{x})^3}{n\delta^3} \tag{32}$$

where n is the number of elements in the testing sample, x_i is value the i^{th} element, and δ is the standard deviation of testing sample, $\overline{x}$ is the arithmetic mean of the sample.

$$kurt\ a_4 = \sum \frac{(x_i - \overline{x})^4}{n\delta^4} \tag{33}$$

Table 4 illustrates that the datasets have a small Skewness rate (0.2227, 0.0965, 0.4882, -0.154269077, 0.4382), which means that the datasets have a normal distribution. Also, the datasets have a small kurtosis value (−0.1201, −1.2817, −1.2334, 2.2020, −1.3033), which indicates a lighter tail than a normal distribution.

Table 4 illustrates the mean value of the experimental data of (temperature, solar irradiance, current, voltage, power) with a norm figure of (31.19 °C, 236.90 W/m^2, 2.79 A, 152.71 V, and 428.64 W) respectively. However, the value of mean presents smaller differences with the amount of median (30.63 °C, 249.38 W/m^2, 2.09 A, 152.32 V, 327.31 W) accordingly. Table 5 shows a high correlation between the output variables (current and power) with a rate of 0.9993, because the power mainly depends on the current value. Also, it shows a moderate correlation between solar irradiation and the output variables (current and power) with a rate of 0.5244.

4.2.3. Neural computing results

The neural predicting models were utilized and implemented using NeuroSolutions software. The experimental data consists of 500 pairs of data sets (Input, Output) used to train and learn the proposed models. The information is recorded every one hour. Figure 9 (a) illustrates the comparison of experimental values of power variable and the predicted output of proposed models (FRNN, PCA), which indicates well fits between the experimental and predicted data based on MSE value of (0.177, 0.078), respectively. Table 6 shows that the proposed models achieved an amount of normalized MSE (NMSE) with a rate of (0.4965, 0.4391), and the value of the correlation rate of (0.7471, 0.7533) accordingly. On the other side, the system rated power in the lab at standard test conditions is 1400 W at 1000 W/m^2, 25 °C, and 1.5 AM.

However, due to the high solar irradiance (G) in Sohar, the power production approach 1102.91 W at 12:00 noon. However, FRNN is better in simulating the experimental results curve comparing with PCA. Figure 9 (b) depicts a comparison of the experimental data of the current variable and the generated output of proposed predicting models (FRNN, PCA), which shows a close relation fitting between the experimental and forecasting data based on MSE value of (0.0488, 0.0768), respectively.

The unsupervised learning starts with assigning random values to weight, and then these weights will stabilize and get the optimal value. This impacts some variations between the desired output and the computed results in the first iterations until the network is stabled and trained. Table 6 shows that the proposed models achieved an amount of NMSE with a rate of (0.4434, 0.4420), and the value of the correlation rate of (0.8119, 0.7623) accordingly. FRNN current waveform is matching the pattern of the measured waveform comparing with PCA.

However, early morning at the beginning of the solar day, there is a bit of difference between measured and predicted values due to the low G. This is because the inverter starts searching for the maximum power point until it reaches the threshold value. This situation makes the measured P_{PV} low, and this is reflected in the predicted values. Table 6 summarized the evaluation factors and results of proposed neural models (FRNN, PCA) for the current and power variables. From R^2 it is found that the predicted current is more accurate using FRNN than PCA. However, P_{PV} is close for FRNN and PCA. From the other side, MSE shows that the prediction model error is less for PCA comparing with FRNN.

The results must compare under the same conditions for the comparison to be accurate and fair. This is missing in most comparisons with previous studies, as most studies are conducted using particular inputs and are calculated under different conditions. Therefore, the comparison is relative to the method type and the accurate evaluation factors.

The comparison with references [21] is relatively sound because it is in the same weather conditions but with a different installation angle for the PV module. Table 7 presents comprehensive evaluations and comparisons of the proposed models' results with other researchers in the literature survey for validating the obtained results.

5. Conclusions

One-year evaluation and comparison of GCPV system performance in Oman based on experiment and two proposed neural prediction models are presented in this paper. Various technical and economic criteria were used to evaluate the effectiveness of the GCPV system. Full recurrent neural network (FRNN) and principal component analysis (PCA) were used to predict the system output. The proposed prediction models used ambient temperature and solar irradiation as input variables. The electrical current and power were predicted, evaluated, and compared with measured values for validation. The highest technical results found yield 5.65 kWh/kWp-day, the capacity factor was 21.7%, and energy production was 245.8 kWh. However, the energy cost was 0.045 USD/kWh, and the payback period was 11.17 years. The two neural prediction

Table 7. The comparison between the proposed models and other studies.

	FRNN	PCA	MFFNN-GA [21]	MFFNN-MVO [21]	Single RNN- SGRU [22]	Multi RNN- MGRU [22]	Bayesian neural [23]	Support vector reg. [23]	Elastic net reg. [23]
MSE	0.1778	0.0780	0.565	0.033	Acc.0.627	Acc.0.529	0.00001	0.2514	0.4761
NMSE	0.4965	0.4391	0.036	0.028	0.1367	0.1118	-	-	-
R^2	0.7471	0.7533	0.9913	0.9992	-	-	0.9999	0.9436	0.8933

models FRNN and PCA achieved 0.0488 and 0.0768 MSE for the current prediction. However, the achieved R^2 is 0.7471 and 0.7533 for power, respectively. It is found that FRNN is better in simulating the experimental results curve comparing with PCA. The information, evaluation, and comparison in this study present a pathway for GCPV system current and power prediction using two essential neural networks (FANN and PCA), considering solar irradiation and ambient temperature variation.

The dependability of such GCPV is a fundamental point for investment, residential, and business applications. Additionally, it fundamental to the viewpoint identified with the future research progress in the direction of evaluating the degree and size of environment impacts condition present on GCPV systems which is essential for further improvement, explicitly in the solar ballet zone and average locales of moderately high ambient temperatures and solar irradiation levels, or general provincial and desert atmospheres.

Declarations

Author contribution statement

Hussein A. Kazem, Jabar H. Yousif, Miqdam T Chaichan, Ali H A Al-Waeli & K Sopian: Conceived and designed the experiments; Performed the experiments; Analyzed and interpreted the data; Wrote the paper.

Funding statement

This work was supported by the Ministry of Higher Education, Research and Innovation (MoHERI) of the Sultanate of Oman under Block Funding Program; MoHERI block Funding Agreement NO ORG SU EI 11 010 and TRC/BFP/SU/01/2018.

Data availability statement

The authors do not have permission to share data.

Declaration of interests statement

The authors declare no conflict of interest.

Additional information

No additional information is available for this paper.

References

[1] P. Singh, V. Mudgal, S. Khanna, T.K. Mallick, K.S. Reddy, Experimental investigation of solar photovoltaic panel integrated with phase change material and multiple conductivity-enhancing-containers, Energy 205 (2020).
[2] A.H.A. Al-Waeli, et al., Comparison study of indoor/outdoor experiments of a photovoltaic thermal PV/T system containing SiC nanofluid as a coolant, Energy 151 (2018) 33–44.
[3] I.M.C. Protogeropoulos, I. Klonaris, C. Petrocheilos, I. Charitos, Performance evaluation of different PV module technologies in a grid-connected pilot project in Greece, in: 25th European Photovoltaic Solar Energy Conference and Exhibition/5th World Conference on Photovoltaic Energy Conversion, 6-10 September 2010, Valencia, Spain, 2010, pp. 4601–4606.
[4] M.B. Shuvho, M.A. Chowdhury, S. Ahmed, M.A. Kashem, Prediction of solar irradiation and performance evaluation of grid connected solar 80 KWp PV plant in Bangladesh, Energy Rep. 5 (2019 Nov 1) 714–722.
[5] A. Chbihi, S. Naamane, S. Boukheir, M. Mouadine, M.H. Bouhamidi, Outdoor investigation of the performance of three PV panels technologies in Morocco, Sol. Energy 220 (2021 May 15) 8–17.
[6] M.E. Dahmoun, B. Bekkouche, K. Sudhakar, M. Guezgouz, A. Chenafi, A. Chaouch, Performance evaluation and analysis of grid-tied large scale PV plant in Algeria, Energy Sustain. Dev. 61 (2021 Apr 1) 181–195.
[7] Y.Y. Wu, S.Y. Wu, L. Xiao, Performance analysis of photovoltaic–thermoelectric hybrid system with and without glass cover, Energy Convers. Manag. 93 (2015) 151–159. .
[8] P.G. Charalambous, G.G. Maidment, S.A. Kalogirou, K. Yiakoumetti, Photovoltaic thermal (PV/T) collectors: a review, Appl. Therm. Eng. 27 (2–3) (2007) 275–286.
[9] H.A. Kazem, T. Khatib, K. Sopian, Sizing of a standalone photovoltaic/battery system at minimum cost for remote housing electrification in Sohar, Oman, Energy Build. 61 (2013) 108–115.
[10] D.T. Cotfas, P.A. Cotfas, D. Ciobanu, O.M. MacHidon, Characterization of photovoltaic-thermoelectric-solar collector hybrid systems in natural sunlight conditions, J. Energy Eng. 143 (6) (2017) 1–10.
[11] S. Mahmoudinezhad, S.A. Atouei, P.A. Cotfas, D.T. Cotfas, L.A. Rosendahl, A. Rezania, Experimental and numerical study on the transient behavior of multi-junction solar cell-thermoelectric generator hybrid system, Energy Convers. Manag. 184 (November 2018) (2019) 448–455.
[12] A.H.A. Al-Waeli, K. Sopian, J.H. Yousif, H.A. Kazem, J. Boland, M.T. Chaichan, Artificial neural network modeling and analysis of photovoltaic/thermal system based on the experimental study, Energy Convers. Manag. 186 (February) (2019) 368–379.
[13] W. Wu, W. Liao, J. Miao, G. Du, Using gated recurrent unit network to forecast short-term load considering impact of electricity price, Energy Proc. 158 (2019) 3369–3374.
[14] A.H.A. Al-Waeli, H.A. Kazem, J.H. Yousif, M.T. Chaichan, K. Sopian, Mathematical and neural network modeling for predicting and analyzing of nanofluid-nano PCM photovoltaic thermal systems performance, Renew. Energy 145 (2020) 963–980.
[15] D.J. Đozić, B.D. Gvozdenac Urošević, Application of artificial neural networks for testing long-term energy policy targets, Energy 174 (2019) 488–496.
[16] X. Kong, X. Xu, Z. Yan, S. Chen, H. Yang, D. Han, Deep learning hybrid method for islanding detection in distributed generation, Appl. Energy 210 (April) (2018) 776–785.
[17] M. Hossain, S. Mekhilef, M. Danesh, L. Olatomiwa, S. Shamshirband, Application of extreme learning machine for short term output power forecasting of three grid-connected PV systems, J. Clean. Prod. 167 (2017) 395–405.
[18] A.A. Du Plessis, J.M. Strauss, A.J. Rix, Short-term solar power forecasting: investigating the ability of deep learning models to capture low-level utility-scale Photovoltaic system behaviour, Appl. Energy 285 (2021 Mar 1) 116395.
[19] K. Wang, X. Qi, H. Liu, A comparison of day-ahead photovoltaic power forecasting models based on deep learning neural network, Appl. Energy 251 (November 2018) (2019) 113315.
[20] L. Wen, K. Zhou, S. Yang, X. Lu, Optimal load dispatch of community microgrid with deep learning based solar power and load forecasting, Energy 171 (2019) 1053–1065.
[21] M. Talaat, T. Said, M.A. Essa, A.Y. Hatata, Integrated MFFNN-MVO approach for PV solar power forecasting considering thermal effects and environmental conditions, Int. J. Electr. Power Energy Syst. 135 (2022 Feb 1) 107570.
[22] Y. Qu, J. Xu, Y. Sun, D. Liu, A temporal distributed hybrid deep learning model for day-ahead distributed PV power forecasting, Appl. Energy 304 (2021 Dec 15) 117704.
[23] S. Chahboun, M. Maaroufi, Principal component analysis and machine learning approaches for photovoltaic power prediction: a comparative study, Appl. Sci. 11 (17) (2021 Jan) 7943.
[24] Y. Sun, V. Venugopal, A.R. Brandt, Short-term solar power forecast with deep learning: exploring optimal input and output configuration, Sol. Energy 188 (June) (2019) 730–741.
[25] X. Qiu, Y. Ren, P.N. Suganthan, G.A.J. Amaratunga, Empirical Mode Decomposition based ensemble deep learning for load demand time series forecasting, Appl. Soft Comput. J. 54 (2017) 246–255.
[26] H.F. Yang, Y.P.P. Chen, Hybrid deep learning and empirical mode decomposition model for time series applications, Expert Syst. Appl. 120 (2019) 128–138.
[27] M. Längkvist, L. Karlsson, A. Loutfi, A review of unsupervised feature learning and deep learning for time-series modeling, Pattern Recogn. Lett. 42 (1) (2014) 11–24.
[28] Y. He, G.J. Mendis, J. Wei, Real-time detection of false data injection attacks in smart grid: a deep learning-based intelligent mechanism, IEEE Trans. Smart Grid 8 (5) (2017) 2505–2516.
[29] S. Wang, S. Fan, J. Chen, X. Liu, B. Hao, J. Yu, Deep-learning based fault diagnosis using computer-visualised power flow, IET Gener., Transm. Distrib. 12 (17) (2018) 3985–3992.
[30] K. Wang, X. Qi, H. Liu, Photovoltaic power forecasting based LSTM-Convolutional Network, Energy 189 (2019) 116225.
[31] H.A. Kazem, J. Yousif, M.T. Chaichan, A.H. Al-Waeli, Experimental and deep learning artificial neural network approach for evaluating grid-connected photovoltaic systems, Int. J. Energy Res. 43 (14) (2019 Nov) 8572–8591.
[32] N.A. Mohammed, M.H. Albadi, Demand response in electricity generation planning, Electr. J. 33 (7) (2020) 106799.
[33] A.H. Al-Badi, M.H. Albadi, A.M. Al-Lawati, A.S. Malik, Economic perspective of PV electricity in Oman, Energy 36 (1) (2011) 226–232.
[34] International Renewable Energy Agency, IRENA_RRA_Oman_2014, 2014.
[35] D.H. Muhsen, M. Nabil, H.T. Haider, T. Khatib, A novel method for sizing of standalone photovoltaic system using multi-objective differential evolution algorithm and hybrid multi-criteria decision making methods, Energy 174 (2019) 1158–1175.
[36] H.A. Kazem, J.H. Yousif, Comparison of prediction methods of photovoltaic power system production using a measured dataset, Energy Convers. Manag. 148 (2017).
[37] W. Hongkang, L. Li, W. Yong, M. Fanjia, W. Haihua, N.A. Sigrimis, Recurrent neural network model for prediction of microclimate in solar greenhouse, IFAC-PapersOnLine 51 (17) (2018) 790–795.

[38] J.H. Yousif, H.A. Kazem, J. Boland, Predictive models for photovoltaic electricity production in hotweather conditions, Energies 10 (7) (2017).
[39] A.A.M.H. Al Asbahi, F.Z. Gang, W. Iqbal, Q. Abass, M. Mohsin, R. Iram, Novel approach of principal component analysis method to assess the national energy performance via energy trilemma index, Energy Rep. 5 (2019) 704–713.
[40] K.G. Sheela, S.N. Deepa, Review on methods to fix number of hidden neurons in neural networks, Math. Probl Eng. 2013 (2013).
[41] A. Tavanaei, M. Ghodrati, S.R. Kheradpisheh, T. Masquelier, A. Maida, Deep learning in spiking neural networks, Neural Network. 111 (2019) 47–63.
[42] A.H. Al-Badi, Measured performance evaluation of a 1.4 kW grid connected desert type PV in Oman, Energy Sustain. Dev. 47 (2018) 107–113.
[43] Y. Zhou, N. Zhou, L. Gong, M. Jiang, Prediction of photovoltaic power output based on similar day analysis, genetic algorithm and extreme learning machine, Energy 204 (2020) 117894.